Materials Advances

ROYAL SOCIETY OF CHEMISTRY

PAPER

View Article Online
View Journal | View Issue

Cite this: *Mater. Adv.*, 2024, 5, 1160

Non-enzymatic amperometric glucose sensing by novel Cu-MOF synthesized at room temperature†

Sondes Guesmi,[a] Kaveh Moulaee,[b] Viviana Bressi,[b] Hamza Kahri,[a] Amani Khaskhoussi,[b] Claudia Espro,[b] Houcine Barhoumi[a] and Giovanni Neri *[b]

Received 14th August 2023,
Accepted 5th December 2023

DOI: 10.1039/d3ma00551h

rsc.li/materials-advances

Cu-metal–organic framework (Cu-MOF) derived from 1,2,4,5-benzene tetracarboxylic acid (H_4BTC) has been synthesized through a quick and soft-template synthesis at room temperature. XRD, FT-IR, BET, SEM-EDX, and Raman spectroscopy were used for the morphological and microstructural characterization. The as prepared Cu-MOF was drop-cast onto a screen-printed carbon electrode (SPCE) for developing a sensitive enzyme-free electrochemical glucose platform. The electrochemical behaviour was investigated by cyclic voltammetry and amperometric tests, highlighting the good electrochemical sensing properties towards glucose detection. A remarkable enhancement was obtained combining Cu-MOF with chitosan (Cs). The Cs/Cu-MOF/SPCE sensor displayed a high sensitivity of 1378.11 μA cm^{-2} mM^{-1} and a low detection limit of 2 μM ($3\sigma/s$) in a linear dynamic range (R^2 = 0.992) from 2 μM to 1700 μM. The practical applicability of the Cs/Cu-MOF/SPCE sensor was evaluated by detecting glucose in spiked saliva samples resulting in a high recovery percentage (ranging from 95.4% to 108.7%). These results, along with the quick and simple synthesis of Cu-MOFs at room temperature, open new routes for developing efficient enzyme-free glucose sensors.

1. Introduction

Glucose is a substance used in the food and fermentation industry. It plays a key role in human life, being the primary energy feed for the body but, if present in large excess in the blood as in people with diabetes, it becomes a concern because may cause several pathologies and increase mortality. Consequently, glucose determination through simple tests in the fields of food, agricultural, biotechnology and medical diagnostics has been largely investigated.[1–3] To address these needs, significant efforts have been directed towards the development of rapid and reliable methods for glucose determination using various sensing technologies including optical,[4] fluorescent,[5] chromatographic,[6] acoustic,[7] and electrochemical.[8]

Among them, electrochemical glucose sensing based on the principle of electro-catalytic glucose oxidation is considered to be an effective method due to its high sensitivity, favorable selectivity, very low detection limit and portability.[9,10] Although enzymatic electrochemical technologies are the most widely commercially available, their broader applications are hindered by the high cost and inherent instability of enzymes.[11] In recent years, non-enzymatic glucose sensors have been developed rapidly, with many advantages such as good long-term stability, convenient operation, and ease of portability.[10] Moreover, these conventional sensors necessitate the extraction of a small blood sample, typically obtained from the fingertip or forearm using a lancet. This method not only makes them invasive but also potentially painful, particularly for diabetic patients who have to undergo multiple daily measurements.[12] Consequently, significant efforts have been directed towards the development of non-invasive alternatives for improving glucose monitoring protocols in diverse human biofluids, such as sweat, tears, saliva, urine, and interstitial fluid.[13] Numerous studies have consistently shown a strong connection between blood glucose levels and the presence of glucose in saliva. Consequently, salivary glucose presents itself as a promising alternative diagnostic tool for diabetes.[14]

In recent years, various nanomaterials have been studied for the electrochemical detection of glucose such as metal (Au, Pt),[15,16] metal alloys (Au–Pt),[17] metal oxides[17–19] (Cu_2O, CuO, and ZnO)[18–20] and metal–organic frameworks (MOFs).[21] Recently, researchers have discovered that MOFs possess large potential in the field of electrochemical sensing. MOFs readily interact with a wide range of molecular targets, thereby also demonstrating a sensing capability for a variety of analytes exhibiting exceptional selectivity and sensitivity.[22] This is primarily attributed to their remarkable characteristics such as a

[a] *Laboratory of Interfaces and Advanced Materials, Faculty of Sciences, University of Monastir, Tunisia*
[b] *Department of Engineering, University of Messina, Messina, Italy. E-mail: giovanni.neri@unime.it*

† Electronic supplementary information (ESI) available. See DOI: https://doi.org/10.1039/d3ma00551h

significantly large specific surface area, variable pore size, and the presence of various functional groups. MOFs are highly porous organic–inorganic materials composed of organic ligands and metal ions (Fe, Zn, Co, *etc.*). MOF synthesis typically requires high temperatures and pressures using solvothermal and microwave techniques.[23] However, room temperature synthesis significantly reduces energy costs and some studies reporting its feasibility were found in the literature. Dang *et al.* successfully prepared a biocompatible Zn-MOF at room temperature in the presence of CTAB and PVP as surfactants.[24] Jin *et al.* reported the preparation of seven MOFs based on cerium at ambient temperature in aqueous solution in the presence of sodium acetate.[25]

Nevertheless, due to their instability in water and low conductivity, MOFs are limited in their use in electrochemical sensors.[26,27] To overcome these limitations, MOFs are combined with other functional materials such as carbon nanotubes,[28] metal nanoparticles,[29] and polymers[30] such as chitosan.[31] The latter is a natural polymer widely used in electrochemical sensing[32,33] due to its attractive proprieties such as biocompatibility, permeability and excellent ability to form conductive and stable films.[34] Taking this into account, chitosan can be a good candidate to immobilize MOFs into the surface of electrodes.

In this paper, a new copper-based metal–organic framework (Cu-MOFs) based on 1,2,4,5-benzene tetracarboxylic acid (H_4BTC), was successfully synthesized using a simple method at ambient temperature. Copper is a transition metal used in many MOF systems for various applications, such as pollutant degradation,[35] heterogeneous catalysis,[36] photocatalysis,[37] many others[38] and gas sensors.[39] Combining the resulting Cu-MOF with chitosan, a Cs/Cu-MOF nanocomposite was formed, leading to an enhanced electrocatalytic activity for glucose oxidation. A screen-printed carbon electrode (SPCE) platform was used and modified to develop a Cs/Cu-MOFs/SPCE sensor for the determination of glucose. The sensor exhibits outstanding features such as a wide linear range, low detection limit, and high sensitivity. Furthermore, the sensor demonstrated remarkable long-term stability and impressive selectivity, which makes capable of detecting glucose in human saliva.

2. Experimental section

2.1 Materials

Copper(II) nitrate trihydrate ($Cu(NO_3)_2\ 3H_2O$), 1,2,4,5-benzene tetracarboxylic acid (H_4BTC), dimethyl sulfoxide (DMSO), trimethylamine (TEA; (C_2H_5)), and polyethylene glycol (PEG, with an average molecular weight of 20 000 g mol^{-1}), potassium hydroxide (KOH), glacial acetic acid (99%), sodium chloride (NaCl), chitosan (Cs), glucose (Glu), dopamine (DA), ascorbic acid (AA), uric acid (UA), mannose, sucrose, fructose, magnesium sulfate ($MgSO_4$), calcium chloride ($CaCl_2$) were purchased from Sigma-Aldrich. All chemicals used in this work were of analytical grade and used as received without further purification. Ultrapure water (18.2 MΩ cm^{-1}) from a Milli-Q ultrapure system was used in this study.

2.2 Synthesis of Cu-MOF

Cu-MOF was prepared using a previously developed procedure.[40] Here is a brief description of the preparation process: first, 0.4 g of PEG was added to 25 mL of DMSO and then, 0.48 g (2 mmol) of $Cu(NO_3)_2 \times 3H_2O$ was added to the solution. The mixture was stirred for 5 minutes to form a suspension solution. In parallel, 0.127 g (0.5 mmol) of H_4BTC was dissolved in 25 mL of DMSO. Additionally, 1.5 mL of triethylamine (TEA), used as a base, was added to create a second mixture solution. Next, the PEG suspension solution (average molecular weight = 20 000 g mol^{-1}) was combined with the second solution, and the mixture was stirred for 10 minutes. During this process, blue colloids started to form. The resulting blue colloids were collected by centrifugation at 3000 rpm for 15 minutes. They were then extracted and washed five times with methanol to remove any remaining undissolved reagents. Finally, the blue-colored Cu-MOF product was dried in a vacuum oven at 423 K for 24 hours.

2.3 Characterization methods

Cu-MOF was characterized by using several techniques such as X-ray powder diffraction (XRD), Fourier infrared spectra (FT-IR), Brunauer–Emmett–Teller (BET), Raman and scanning electron microscopy with energy dispersive X-ray spectroscopy (SEM-EDX). XRD characterization was performed using a Bruker D8 Advance A25 X-ray diffractometer, operating at 40 kV and in the range 5–80° (2θ), with an increasing rate of 0.01° s^{-1} using the CuKa1 radiation. FTIR spectra were obtained using a PerkinElmer spectrometer, equipped with a universal ATR sampling accessory, performed in the range from 4000 to 500 cm^{-1} at room temperature with a scanning speed of 2 mm s^{-1}, resolution of 4.0 cm^{-1} and accumulation scan of 30. BET surface area and porosity of samples were evaluated by nitrogen adsorption and desorption isotherms carried out at 77 K using a Quantachrome® ASiQwin™ instrument (Anton Paar Companies). SEM images were obtained using a Zeiss CrossBeam 540 microscope, which was equipped with an EDX detector. Raman spectra were recorded at room temperature using a HORIBA (HR800) micro-spectrometer. Before starting the measurements, the samples were dried and degassed under vacuum overnight. The used experimental conditions are 1200 grating, 30 seconds, 5 accumulations, objective (100×), and power 1.6 mW.

2.4 Modified electrode fabrication and electrochemical tests

Screen-printed carbon electrodes (mod C110) were purchased from DropSens (Metrohm). To modify the bare SPCE, a dispersion of 5 mg of synthesized Cu-MOF in 1 mL of distilled water was fabricated through sonication for 30 minutes in an ultrasonic bath. Subsequently, 15 μL of this suspension was carefully drop-cast onto the surface of the working carbon electrode and left to dry at room temperature overnight. The sensor was also modified by drop casting a Cu-MOF mixture with 0.2%

chitosan stock solution (15% v/v), so the Cs/Cu-MOF composite was obtained. The modified sensors were characterized using various techniques. Cyclic voltammetry (CV) and chronoamperometry analyses were performed using a DropSens μStat 400 potentiostat, along with the Dropview 8400 software for data acquisition. The tests were carried out in a KOH solution, at a scan rate of 50 mV s^{-1} and in a potential range from 0 to 1 V. The concentration of the investigated analyte (glucose) was varied to study the electrochemical behavior of the modified sensors. To determine the limit of detection (LOD), calibration curves were generated by plotting the faradaic current against the analyte concentration. The sensitivity was calculated as the slope of the calibration curve obtained.

2.5. Preparation of real samples

Before meals, saliva samples were obtained from healthy individuals and collected in Eppendorf tubes, following the standard protocol for diabetes analysis.[41] These samples were then diluted 100-fold with a 0.05 M KOH solution. After dilution, known concentrations of glucose were added to the samples. The recoveries of glucose were calculated to validate the sensor performance.

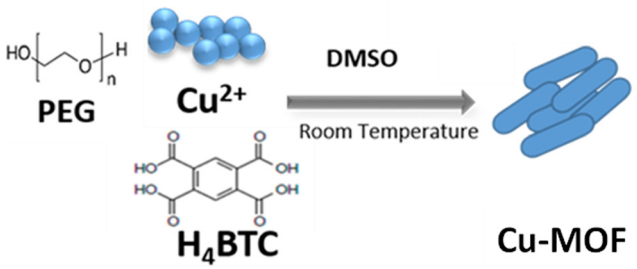

Scheme 1 Preparation process of Cu-MOF.

3. Results and discussion

3.1 Synthesis and characterization of Cu-MOF

Cu-MOF containing the H_4BTC ligand was synthesized according to the method described in detail above. A schematic view of the preparation of Cu-MOF is reported in Scheme 1.

A view of the possible Cu-MOF network structure synthesized, designed by means of the VESTA software, is reported in (Fig. 1a), highlighting the capability of multi-dentate H_4BTC ligand to coordinate Cu ions.

The morphological and microstructural characteristics of the Cu-MOF were investigated by SEM, XRD and Raman analysis. SEM image (Fig. 1b) shows agglomerated flake and rod-like particles of variable sizes ranging approximately from 100 nm to 2 μm. The XRD spectrum (Fig. 1c) exhibits diffraction peaks which are consistent with the ones observed in similar Cu-MOF composites reported in previous studies.[43–45] The low intensity of the reflection peaks suggests that the synthesized Cu-MOF is predominantly amorphous, which can be attributed to the room temperature synthesis and the subsequent low temperature treatment (drying at 423 K). Raman spectrum (Fig. 1d) shows numerous peaks in the range 200–600 cm^{-1}

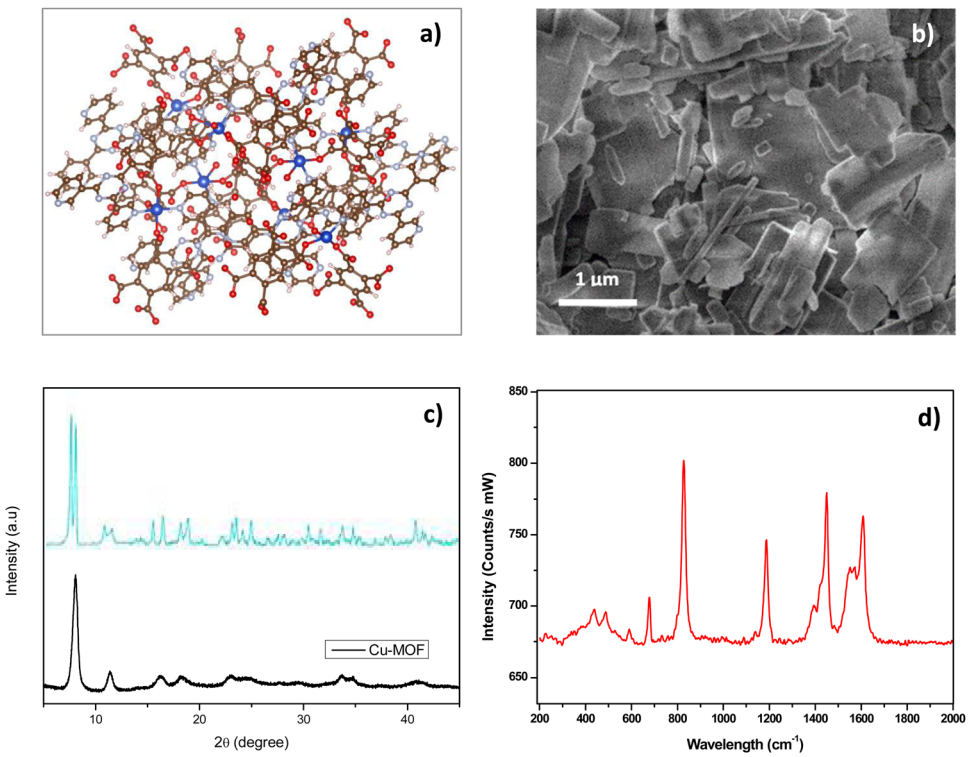

Fig. 1 (a) Possible structure of Cu-MOF by VESTA software (Cu: blue, C: brown, O: sky blue, H: red); (b) SEM mage of Cu-MOF; (c) XRD pattern of Cu-MOF (black curve) compared to pattern (blue curve) described in ref. 42. (d) Raman spectrum of Cu-MOF.

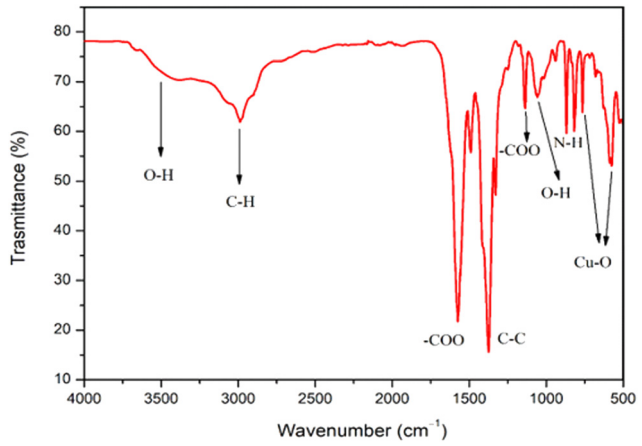

Fig. 2 FTIR spectrum of Cu-MOF.

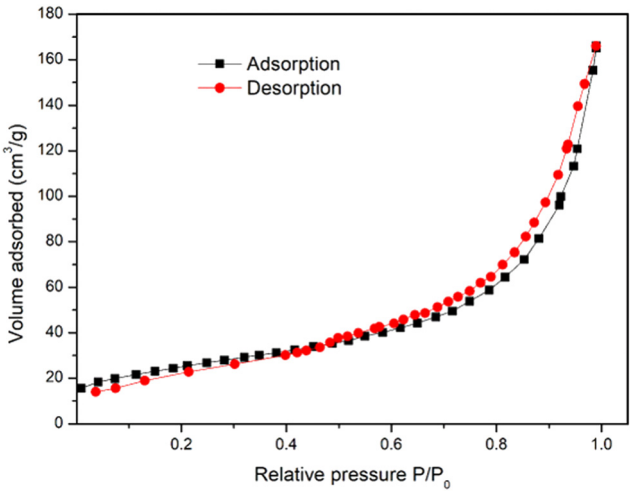

Fig. 3 N_2 adsorption/desorption isotherms of Cu-MOFs.

attributed to Cu–O vibrations modes in the framework structure. The large bands at 827 cm^{-1} and 1190 cm^{-1} are related to vibrations associated with benzene rings of the organic component as well as the larger doublets centered at around 1400 and 1600 cm^{-1}, assigned to carboxyl groups.[46]

The analysis of functional groups on the surface of Cu-MOF was investigated by FT-IR spectroscopy (Fig. 2). The bands around 3500–3300 cm^{-1} are assigned to stretching and bending vibrations of the –OH group.[10] The –OH bending of the hydroxyl group is also visible around 1070 cm^{-1}. Vibration bands at 2980 and 2910 cm^{-1} are assigned to C–H stretching.[47] The large vibration bands for the carboxylic acid function could be observed in the region of 1720–1400 cm^{-1}.

The absorption bands located at 1571 and 1375 cm^{-1} can be assigned to the –COO asymmetric stretching, whereas peaks at 1430 and 1325 cm^{-1} can be assigned to –COO symmetric stretching. In addition, the band at 1640, 1588, and 1374 cm^{-1} could be ascribed to the stretching of $–COO^-$ and the peak at about 1449 cm^{-1} could be assigned to the stretching of C–C on the benzene ring.[47] The peaks around 800 cm^{-1} could be attributed to NH_2 derived from TEA. Furthermore, the spectrum shows the characteristic bands of the Cu–O stretching vibrations at 590 and 766 cm^{-1}.

Textural properties were assessed by BET analysis. The N_2 adsorption/desorption isotherm of Cu-MOF is reported in Fig. 3, showing a type-IV isotherm, which suggests the existence of a range of pore sizes. At medium relative pressures in the range 0.6–0.9 of relative pressure, a hysteresis between adsorption and desorption curves demonstrates the presence of surface pores. The surface area and the average pore diameter of the Cu-MOF were determined to be 61.86 $m^2 g^{-1}$ and 4.31 nm, respectively.

3.2 Characterization of modified-SPCE

Commercial SPCE supports were used to fabricate the modified electrodes, named Cs/SPCE, Cu-MOF/SPCE, and Cs/Cu-MOF/SPCE, printing a layer of the corresponding material on the carbon working electrode. The morphology of the different electrodes is reported in Fig. 4.

SEM images of the chitosan modified electrode revealed a smooth, nonporous membrane layer (Fig. 4a). For Cu-MOF/SPCE, the agglomeration of Cu-MOF particle morphology is clearly noted (Fig. 4b). SEM analysis (Fig. 4c) of the Cs/Cu-MOF/SPCE prove that the chitosan aqueous solution favors the dispersion of Cu-MOF nanorods. This finding strongly indicates that chitosan serves as an effective agent in preventing the agglomeration of Cu-MOF particles. EDX (Fig. 4g–i) and Raman analysis (Fig. 4l–n) provide further evidence for the successful modification of the SPCE electrode with the named modifiers.

3.3 Electrochemical behavior of modified electrodes

The electrochemical behavior of fabricated electrodes was studied by cyclic voltammetry (CV). The measurements were conducted with a solution of 5 mM $K_3[Fe(CN)_6]$ in 0.1 M KCl as the electrolyte. Fig. 5 shows the cyclic voltammograms of the redox probe using the bare SPCE and modified Cs/SPCE, Cu-MOF/SPCE and Cs/Cu-MOF/SPCE. On bare SPCE a redox couple was observed at −126 mV (reduction peak) and 306 mV (oxidation peak) with a peak-to-peak separation, Δ_p, of = 432 mV. CV of the Cu-MOF/SPCE shows a redox couple of lower intensity at 483 and 550 mV (Δ_p = 67 mV). The smaller peak-to-peak separation is likely due to the faster reaction rate of the redox probe at the electrode surface.

It is noteworthy that a large enhancement (more than 5 times) of the anodic and cathodic peak current occurred on the Cs/Cu-MOF/SPCE sensor. The behavior observed derives from the improvement of conductivity of the MOF after chitosan addition which improves the speed of electron transfer.[48,49] Furthermore, chitosan can provide the formation of more catalytically active sites, and increase the stability of the MOF material on the electrode surface, preventing the aggregation of particles of MOFs.[48,50]

Then, the performances of the sensors were evaluated by cyclic voltammetry in the presence of glucose in alkaline medium, which are well known conditions necessary to provide

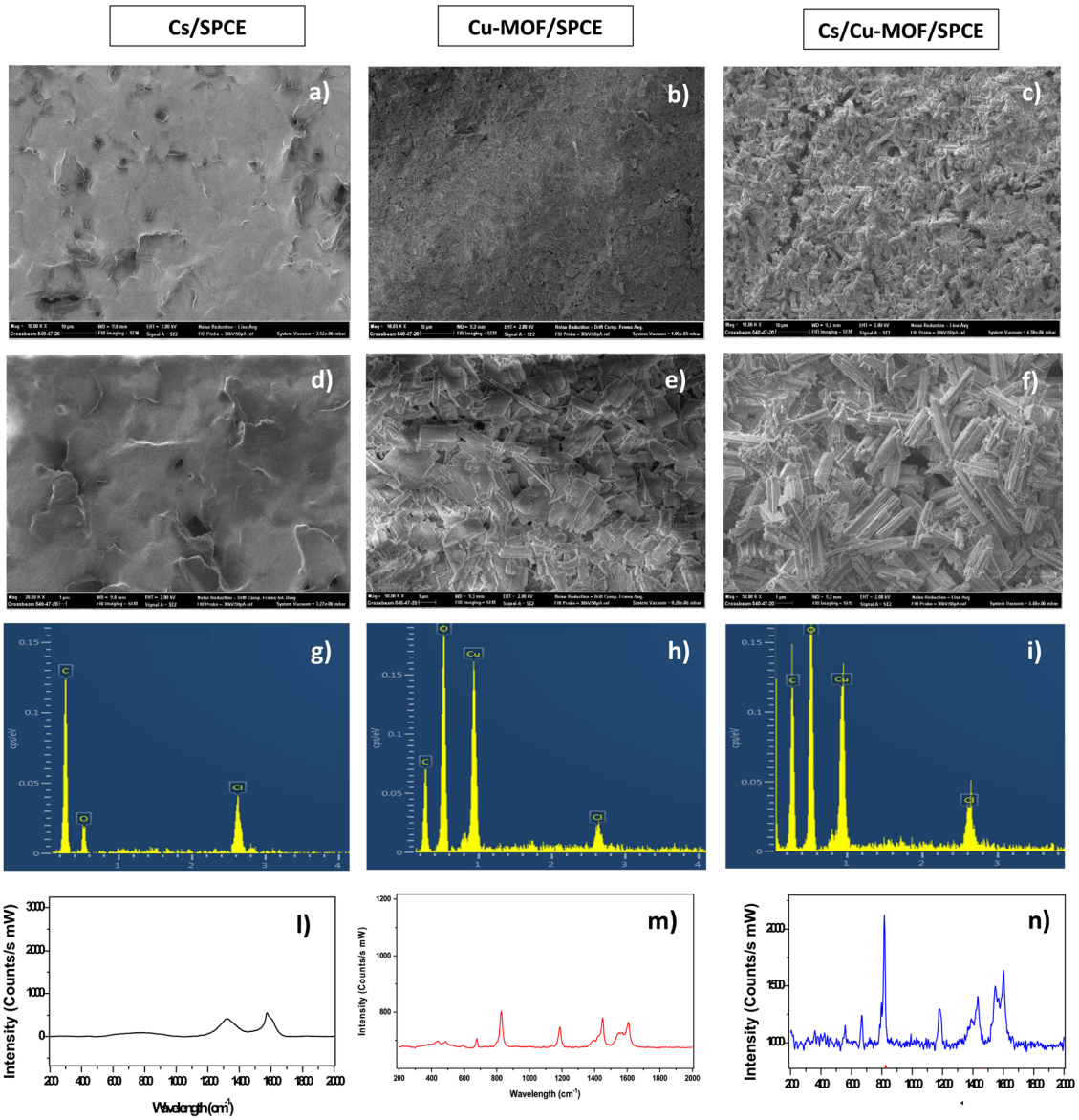

Fig. 4 (a)–(c) SEM images of Cs/SPCE, Cu-MOF/SPCE, and Cs/Cu-MOF taken at low magnification (10 μm), respectively; (d)–(f) SEM images of Cs/SPCE, Cu-MOF/SPCE, and Cs/Cu-MOF taken at high magnification (1 μm), respectively; (g)–(i) EDX analyses; and (l)–(n) Raman spectra.

the electroactive sites for the glucose oxidation on Cu-based sensors.[39] This has been confirmed also for the Cu-MOF/SPCE sensor, as demonstrated by results obtained in KOH at different concentrations (see Fig. S1, ESI†). KOH concentration in the range 0.05–0.1 M resulted provide the best performances and subsequent tests were therefore carried out in these conditions.

Based on these findings, the catalytic mechanism for glucose oxidation at the composite modified electrode is thought to follow the equation[51,52]

$$\mathrm{Cu(II)MOF} + 2\mathrm{OH}^- \rightarrow \mathrm{Cu(III)MOF} + \mathrm{e}^- \quad (1)$$

$$\mathrm{Cu(III)MOF} + \mathrm{glucose} \rightarrow \mathrm{Cu(II)MOF} + \mathrm{gluconolactone} \quad (2)$$

The Cu(II) sites are transformed in the Cu(III) sites, serving as the sites where the glucose molecules are oxidized. The chitosan layer presents in the Cs/Cu-MOF layer acts as a charge transfer layer, which helps in the electron transfer between the Cu(II)/Cu(III) sites and the electrode surface.

Fig. 6 displays the behavior of 200 μM of glucose at different electrodes in 0.05 M KOH solution at a scan rate of 50 mV s^{-1}. For the bare SPCE and Cs/SPCE, no clear peak appeared in the presence of glucose, while an oxidation peak around 0.6 V was observed for both the Cu-MOF/SPCE and Cs/Cu-MOF/SPCE. The glucose oxidation current for the different electrodes is reported in Fig. 7b, which highlights the larger response of the Cs/Cu-MOF/SPCE sensor to glucose compared to other ones. This finding confirms that the Cu-MOF layer has a good electrocatalytic activity for glucose oxidation, which is strongly enhanced by adding chitosan.

The significantly higher current response of the composite Cs/Cu-MOF modified electrode to glucose as compared to Cu-MOF can be attributed to several factors, in addition to the

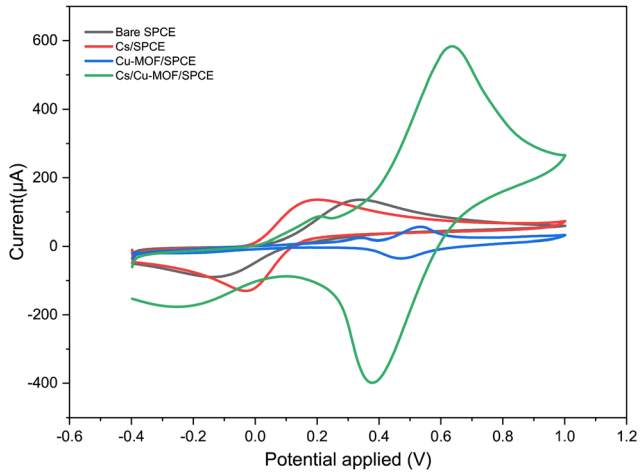

Fig. 5 CVs of Cs/SPCE, Cu-MOF/SPCE, Cs/Cu-MOF/SPCE and bare electrodes in 5 mM $K_3[Fe(CN)_6]$ and 0.1 M KCl.

already cited higher conductivity of chitosan. Firstly, the composite Cs/Cu-MOF structure appears to be more dispersed on the working electrodes, as revealed by SEM analysis, and this leads to a higher surface area. Secondly, the strong film-forming ability of chitosan is advantageous in holding the Cu-MOF electrocatalyst in close proximity to the electrode surface, preventing the leaching and thereby, leading to a stable and high response.[31] Indeed, we observed a noticeable improvement in repeatability (in consecutive measurements) upon the inclusion of chitosan, in comparison to Cu-MOF/SPCE (data not shown).

CVs were recorded at various scan rates, from 25 mV s^{-1} to 1500 mV s^{-1}, in 0.05 M KOH containing 1 mM of glucose. Fig. S2a (ESI†) shows that the anodic peak current displays an increment with a rise in the potential scan rate. Furthermore, the anodic peak is observed to shift positively, indicating a kinetic restriction in the electrochemical oxidation process of glucose.[10] As shown in Fig. S2b (ESI†), the electrocatalytic current of the oxidation peak is directly related to the square root of the scan rate, as per the equation i_{pa} (μA) = $4.91\sqrt{v} + (-2.03)$, where i_{pa} represents the anodic peak current and $\sqrt{v}$ represents the square root of the scan rate with the R^2 value of 0.9932. These findings suggest that slow diffusion of species towards or away from the electrode surface controls the rate-determining step, while adsorption occurs at a faster rate than diffusion, as previously noted.[9]

Additional CV experiments were performed to evaluate its electrochemical activity with respect to different concentrations of glucose in 0.05 M KOH at a scan rate of 50 mV s^{-1}. As can be seen from the graph in Fig. 7a, a clear increase in anodic peak current was observed as the glucose concentration increased from 30 μM to 1.7 mM.

A linear correlation was observed between the anodic peak current and the glucose concentrations, as shown in Fig. 7b. This correlation was modeled using the equation $y = 0.144x + 39.125$ with $R^2 = 0.9922$. Additionally, it was found that as glucose concentrations increased, the anodic peaks shifted to a higher potential (more positive), which may be due to the restriction of glucose diffusion on the surface of the Cs/Cu-MOF electrode.[10] These results confirm that the Cs/Cu-MOF composite exhibits excellent catalytic performance for the oxidation of glucose.

3.4. Amperometric detection of glucose

To ensure maximum sensitivity for our proposed sensor, we utilized the amperometric technique for glucose measurement, as it is known for its rapid and precise detection of low analyte concentrations.[53] To begin, we focused our attention on optimizing the applied potential at the Cs/Cu-MOF/SPCE sensor, as this parameter significantly impacts the current response. The amperometric current–time curves of the Cs/Cu-MOF/SPCE were recorded in 0.05 M KOH, with the successive addition of 100 μM glucose at four different applied potentials: 0.5 V, 0.6 V, 0.7 V, and 0.8 V (Fig. 8a). Following the effect of the applied potential, we noted that the current response increased from 0.5 V to 0.7 V, but then decreased from 0.7 V to 0.8 V. The highest sensitivity was obtained at 0.7 V (Fig. 8b). Consequently, we selected 0.7 V as the optimal value of the applied potential for further experiments.

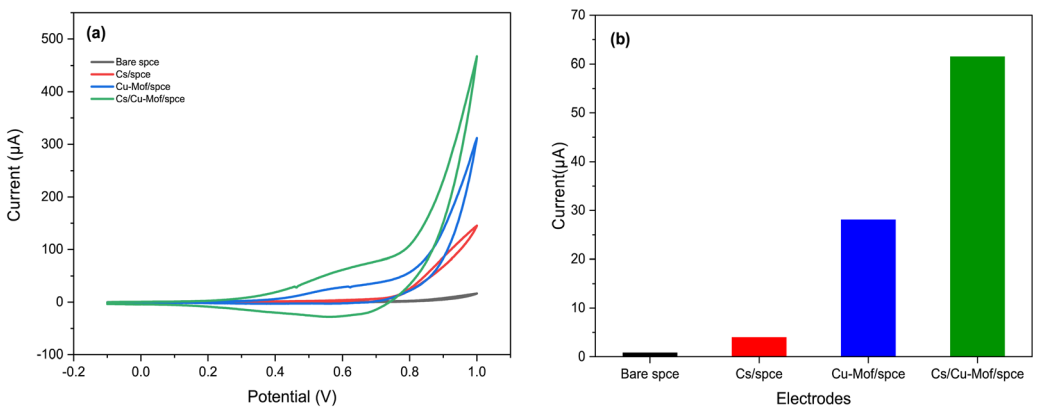

Fig. 6 (a) CVs of the bare SPCE, Cs/SPCE, Cu-MOF/SPCE and Cs/Cu-MOF/SPCE in 0.05 M KOH containing 200 μM glucose at scan rate 50 mV s^{-1}. (b) Comparison of the current oxidation peak of glucose at different sensors.

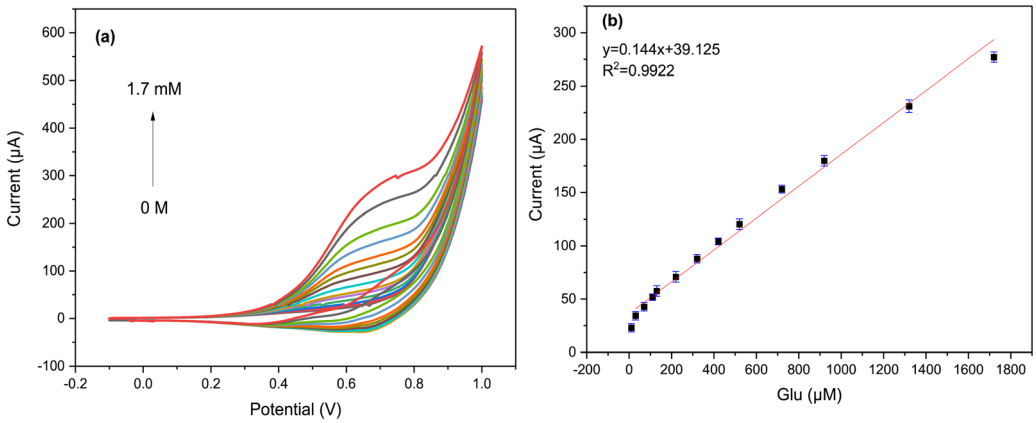

Fig. 7 (a) CVs of Cs/Cu-MOF modified SPCE for different concentrations of glucose (0–1.7 mM) in 0.05 M KOH at a scan rate of 50 mV s^{-1}; (b) the correspondence plots of anodic peak currents *vs.* glucose concentration.

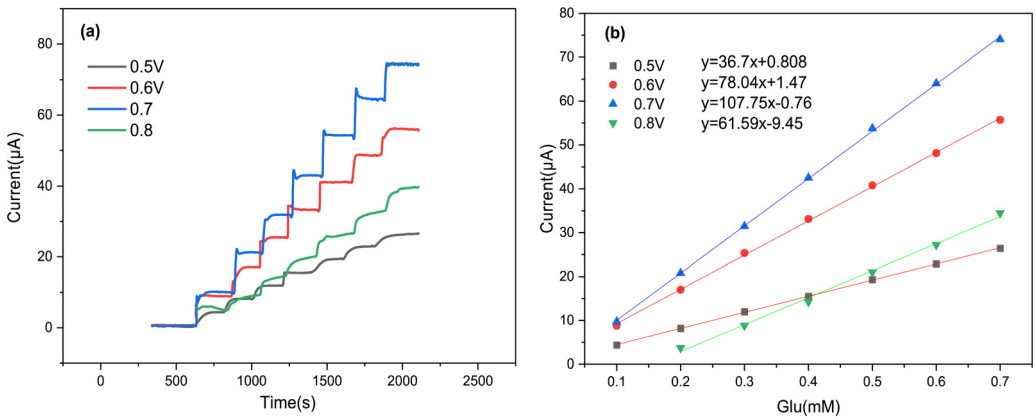

Fig. 8 (a) Amperometric response of the Cs/Cu-MOF/SPCE at different potentials (from 0.5 to 0.8 V) after glucose additions; (b) corresponding calibration curve for each potential.

At the optimum potential, Fig. 9 displays amperometric response of Cs/Cu-MOF electrode towards successive addition of glucose in 0.05 M KOH. Upon addition of glucose, the modified membrane exhibits significant current peaks, where the Cs/Cu-MOF/SPCE demonstrates a linear response in the range of 2 μM to 1.7 mM (R^2 = 0.992) with sensitivity of 173.09 μA mM^{-1} (1378.11 μA cm^{-2} mM^{-1}). The LOD of the Cs/Cu-MOF/SPCE was calculated to be 2 μM using a calibration curve and considering formula $3\sigma/s$, where σ is standard deviation of replicative measurements of blank solution and s is the slope of the calibration curve.

Compared to the recently reported nanomaterials MOF enzyme-free electrochemical glucose sensors listed in Table 1, the Cs/Cu-MOF composite electrode is noteworthy for exhibiting similar levels of sensitivity, detection limit, and range.

3.5. Interference analysis

One of the crucial analytical challenges for glucose sensors is their ability to provide a selective response. Due to the complexity of biological samples, many interfering substances may coexist with glucose, leading to inaccurate glucose measurements. First, we evaluate the effect of some common electrolytes, like Na^+, K^+, Mg^{2+} and Ca^{2+} ions. Fig. 10a shows results for Na^+, demonstrating that also a larger excess of these species does not interfere with the measurements. Then, we evaluated the selectivity of the Cs/Cu-MOF electrode towards other electroactive biomolecules such as fructose, sucrose, mannose (at 10 μM), ascorbic acid, dopamine, uric acid (at 20 μM). These interfering species were added after a first glucose addition of 200 μM at the beginning of the test, carried out in 0.05 M KOH at 0.7 V using the amperometric method; a second addition of glucose was done at the end of the experiment. Fig. 10b demonstrates that glucose measurement is only slightly affected by simple sugars (sucrose, mannose, and fructose) whereas uric acid, dopamine, and ascorbic acid exhibit very low interference effects. These results indicate that the Cs/Cu-MOF/SPCE sensors display a high selectivity, which is an advantage when it is utilized for quantifying glucose in real and complex physiological fluids like blood, saliva, and urine.

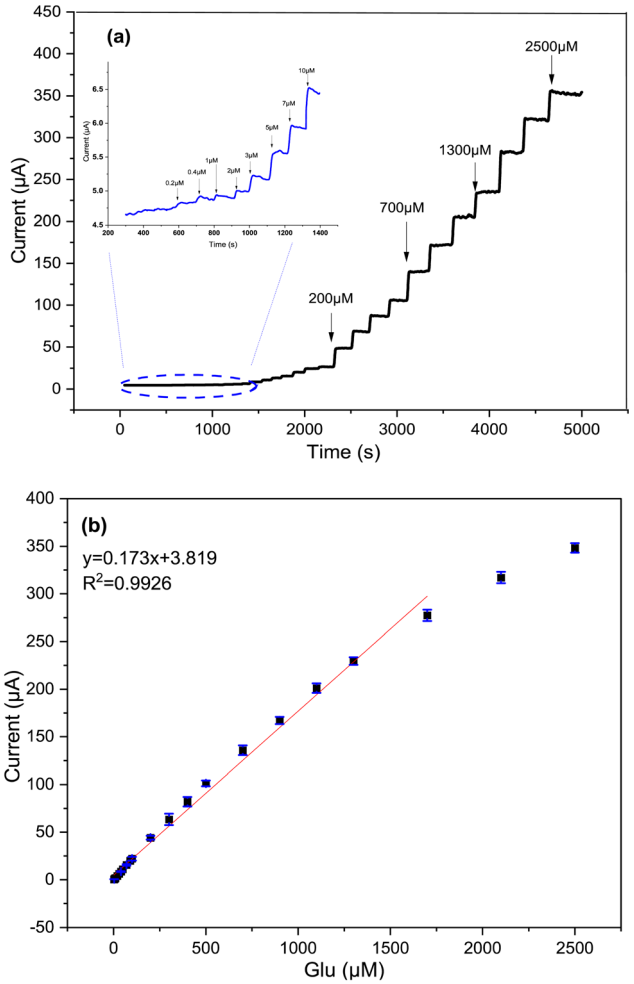

Fig. 9 (a) Amperometric current–time curve of the electrodes of Cs/Cu-MOF/SPCE upon the successive addition of glucose *vs.* Ag/AgCl holding at 0.7 V in 0.05 M KOH; (b) corresponding calibration curve of current vs glucose concentration.

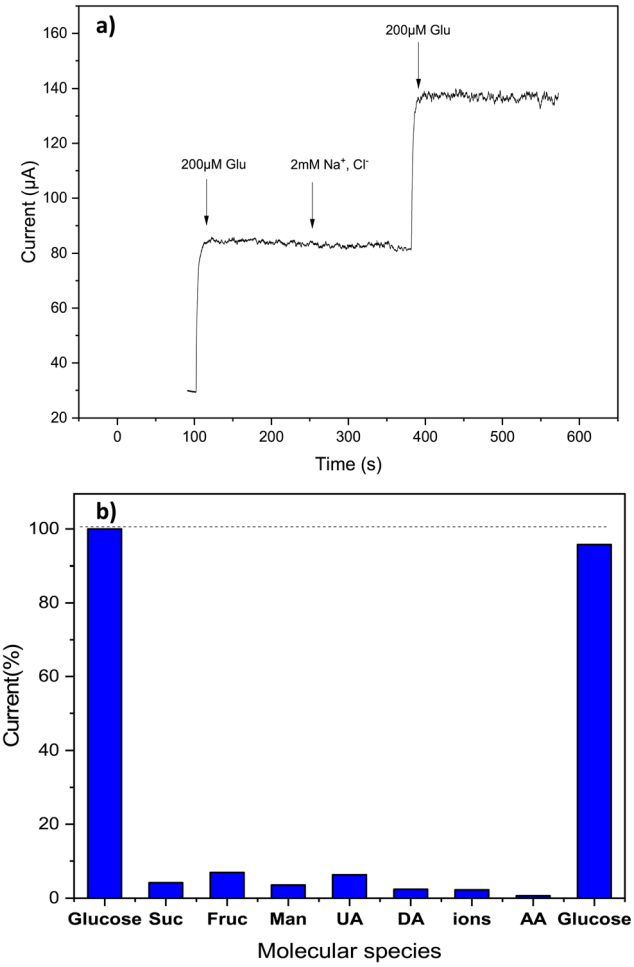

Fig. 10 (a) Chronoamperometry of 200 μM glucose in standard conditions (0.05 M KOH at 0.7 V) and in the presence of a large excess of Na^+ ions; (b) response of Cs/Cu-MOF modified electrode in 0.05 M KOH at 0.7 V to glucose to different interfering biomolecules.

3.6. Stability, repeatability, and reproducibility of Cs/Cu-MOF/SPCE

Repeatability, reproducibility and stability are equally important parameters as selectivity for ensuring the reliable application of electrochemical sensors. Therefore, these parameters of the proposed sensor were examined. As shown in Fig. 11a, a very good repeatability for three different measurements using the same Cs/Cu-MOF/SPCE sensor was obtained. To test the long-term stability of the prepared sensor, the Cs/Cu-MOF/SPCE electrode was stored at room temperature after rinsing with ultra-pure water. The comparison of the current

Table 1 Comparison of different metal-based nanomaterials for electrochemical glucose sensors

Electrode materials	Applied potential (V)	Linear range	Sensitivity (μA cm^{-2} mM^{-1})	LOD (μM)	Ref.
CuO/GCE	0.5	0.5 μM–5 mM	—	0.07	54
HKUST3-1/KSC800	0.45	0.15 μM–5.62 mM	28.67	4.8	55
Cu-MOF@Nafion/GCE	0.5	0.06 μM–5 mM	—	0.01	52
Cu@ Ni MOF/GCE	0.54	0–5 mM	496	0.4	56
SWCNTs-MPsLCu-MOF/GCE	0.31	0.02 μM–0.08 mM	573	0.00172	51
Ni/Co(HHTP)MOF/CC	0.5	0.3 μM–2.312 mM	3250	0.1	10
NiCu-MOF-6	0.55	20 μM–4.93 mM	1832	15	57
Ni-Mof/Ni/NiO/GCE	0.65	0.4 μM–0.9 mM	2133.5	0.1	26
Nafion/Co/MnO@HC/GCE	0.65	Up–6.9 mM	233.8	1.31	58
Co-Mof@CNTs/Nafion/GCE	0.3	10 μM–5 mM	732.94	3	11
MIL-53(NiFe)/Ni	0.6	2 μM–1.6 mM	41.95	0.67	59
Cs/Cu-MOF/SPCE	0.7	2 μM to 1.7 mM	1378.11	2	This work

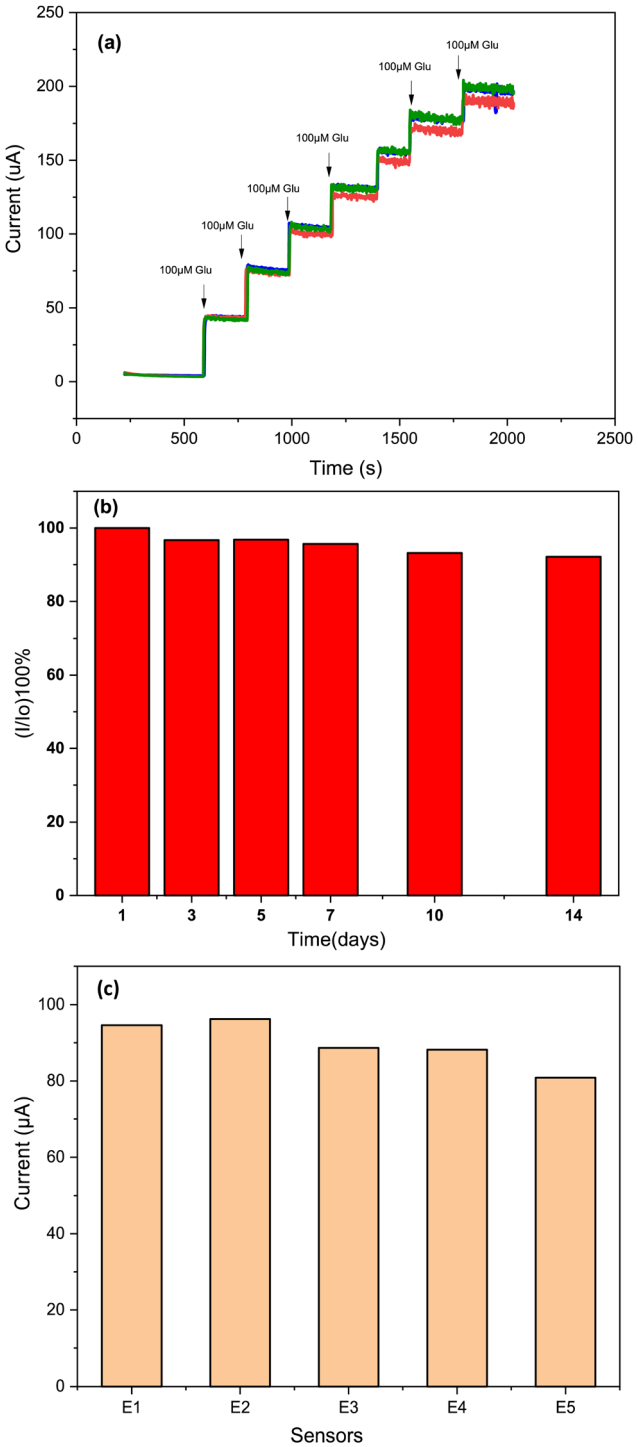

Fig. 11 (a) Repeatability study after successive addition of 100 μM glucose by same electrode, (b) stability during 14 days, and (c) reproducibility of 5 Cs/Cu-MOF sensor measurements in 0.05 M KOH.

measurements of 200 μM taken on the 1st, 5th, 7th, 10th, and 14th days is illustrated in Fig. 11b. The electrode retained 92.16% of its initial response after 14th day, indicating good long-term stability of the Cs/Cu-MOF/SPCE sensor.

Finally, to test the reproducibility of the Cs/Cu-MOF/SPCE sensor, five electrodes were prepared under the same preparation conditions, and the amperometry response of each sensor was recorded (Fig. S3, ESI†) for a glucose concentration of 0.2 mM. The comparison of the bar graph of the four prepared sensors is presented in Fig. 11c, indicating favorable reproducibility.

Table 2 Determination of the glucose levels in spiked human saliva samples

Added (μM)	Found (μM)	Recovery (%)
0	25	—
26	25.8	99.8
66	63	95.4
166	174	104.8
366	398	108.7
766	794	103.4

3.7. Real sample analysis

The development of non-invasive glucose monitoring devices has been a significant research area aimed to enhance the quality of life for diabetic patients. These devices offer a comfortable and safe method of glucose monitoring without the need for invasive procedures that can cause pain and discomfort.[49] To evaluate the applicability of Cs/Cu-MOF/SPCE in the field of non-invasive glucose detection, the constructed sensor was used to evaluate the glucose levels in human saliva samples. Prior to measurement, the human saliva was collected before meals and subsequently diluted 100 times using 0.05 M KOH. The recovery values for the assay of known concentrations of glucose added are calculated to be between 95.4% and 108.7% (see Table 2).

4. Conclusions

To summarize, a novel copper-based metal–organic framework was successfully synthesized for the first time using a quick and simple method at room temperature, utilizing PEG as a template. Cu-MOF modified glassy carbon electrode exhibited promising electrocatalytic properties for glucose detection. The addition of chitosan enhances the electroanalytical performances of the Cu-MOF-Cs in terms of sensitivity and stability. The Cs/Cu-MOF/SPCE sensor demonstrated linear dynamic range concentration 2 μM to 1.7 mM with a low detection limit of about 2 μM, excellent sensitivity (1378.11 μA cm^{-2} mM^{-1}) and good selectivity. The developed sensor was applied for glucose detection in real medium which allows high recovery rate in human saliva samples from 95.4% to 108.7%. These outcomes highlight the significant potential of the proposed sensor for accurate glucose determination in practical applications.

Conflicts of interest

There are no conflicts to declare.

References

1 A. L. Galant, R. C. Kaufman and J. D. Wilson, *Food Chem.*, 2015, **188**, 149–160.
2 D. Bamgboje, I. Christoulakis, I. Smanis, G. Chavan, R. Shah, M. Malekzadeh, I. Violaris, N. Giannakeas, M. Tsipouras, K. Kalafatakis and A. Tzallas, *Biosensors*, 2021, **11**, 189.
3 E. Sehit and Z. Altintas, *Biosens. Bioelectron.*, 2020, **159**, 112165.
4 S. Qasemi and M. Ghaemy, *Int. J. Biol. Macromol.*, 2020, **151**, 901–908.
5 Y. Kim, G. Jang, D. Kim, J. Kim and T. S. Lee, *Polym. Chem.*, 2016, **7**, 1907–1912.
6 W.-Q. Xie, Y.-X. Gong and K.-X. Yu, *J. Chromatogr. A*, 2017, **1520**, 143–146.
7 I. Bayrakli and Y. K. Erdogan, *Opt. Laser Technol.*, 2018, **102**, 180–183.
8 Y. Li, M. Xie, X. Zhang, Q. Liu, D. Lin, C. Xu, F. Xie and X. Sun, *Sens. Actuators, B*, 2019, **278**, 126–132.
9 M. S. Jagadeesan, K. Movlaee, T. Krishnakumar, S. G. Leonardi and G. Neri, *J. Electroanal. Chem.*, 2019, **835**, 161–168.
10 Z. Xu, Q. Wang, H. Zhangsun, S. Zhao, Y. Zhao and L. Wang, *Food Chem.*, 2021, **349**, 129202.
11 Y.-Q. Xie, S.-W. Zong, L. Lu and K.-L. Zhang, *Polyhedron*, 2022, **226**, 116095.
12 D. Bruen, C. Delaney, L. Florea and D. Diamond, *Sensors*, 2017, **17**, 1866.
13 W. Villena Gonzales, A. T. Mobashsher and A. Abbosh, *Sensors*, 2019, **19**, 800.
14 W. Zhang, Y. Du and M. L. Wang, *Sens. Bio-Sens. Res.*, 2015, **4**, 23–29.
15 F. Sun, X. Wang, Z. You, H. Xia, S. Wang, C. Jia, Y. Zhou and J. Zhang, *J. Mater. Sci. Technol.*, 2022, **123**, 113–122.
16 D. Kuang, W. Yu, J. Liu, Y. Yin and C. Wang, *Microchem. J.*, 2023, **191**, 108760.
17 R. Wang, X. Liu, Y. Zhao, J. Qin, H. Xu, L. Dong, S. Gao and L. Zhong, *Microchem. J.*, 2022, **174**, 107061.
18 C. Espro, S. Marini, D. Giusi, C. Ampelli and G. Neri, *J. Electroanal. Chem.*, 2020, **873**, 114354.
19 J. Yang, H. Chen, C. Zhu, Z. Huang, R. Ou, S. Gao and Z. Yang, *Anal. Biochem.*, 2022, **656**, 114857.
20 M. Waqas, C. Liu, Q. Huang, X. Zhang, Y. Fan, Z. Jiang, X. Wang and W. Chen, *Electrochim. Acta*, 2022, **410**, 140040.
21 Y. Wei, Y. Hui, X. Lu, C. Liu, Y. Zhang, Y. Fan and W. Chen, *J. Electroanal. Chem.*, 2023, **933**, 117276.
22 T. Ma, H. Li, J.-G. Ma and P. Cheng, *Dalton Trans.*, 2020, **49**, 17121–17129.
23 J. G. Flores, E. Sánchez-González, A. Gutiérrez-Alejandre, J. Aguilar-Pliego, A. Martínez, T. Jurado-Vázquez, E. Lima, E. González-Zamora, M. Díaz-García, M. Sánchez-Sánchez and I. A. Ibarra, *Dalton Trans.*, 2018, **47**, 4639–4645.
24 Y. T. Dang, M.-H. D. Dang, N. X. D. Mai, L. H. T. Nguyen, T. B. Phan, H. V. Le and T. L. H. Doan, *J. Sci.: Adv. Mater. Devices*, 2020, **5**, 560–565.
25 H.-G. Jin, J.-X. Gu, W. Lin, W.-J. Xu, B.-X. Huang, F. Yang, J.-X. Wen, Y. Ren and Z.-S. Chao, *Microporous Mesoporous Mater.*, 2022, **346**, 112257.
26 J. Chen, Q. Xu, Y. Shu and X. Hu, *Talanta*, 2018, **184**, 136–142.
27 M. Ataei Kachouei, S. Shahrokhian and M. Ezzati, *Sens. Actuators, B*, 2021, **344**, 130254.
28 X. Zhang, Y. Xu and B. Ye, *J. Alloys Compd.*, 2018, **767**, 651–656.
29 S. A. Hira, S. Nagappan, D. Annas, Y. A. Kumar and K. H. Park, *Electrochem. Commun.*, 2021, **125**, 107012.
30 Y. Wang, L. Wang, W. Huang, T. Zhang, X. Hu, J. A. Perman and S. Ma, *J. Mater. Chem. A*, 2017, **5**, 8385–8393.
31 L. Zhang, M. Sun, T. Jing, S. Li and H. Ma, *Colloids Surf. Physicochem. Eng. Asp.*, 2022, **648**, 129225.
32 A. Pandey and A. N. Raja, *Int. J. Biol. Macromol.*, 2020, **164**, 4231–4244.
33 P. Sundaresan, C.-C. Fu, S.-H. Liu and R.-S. Juang, *Colloids Surf. Physicochem. Eng. Asp.*, 2021, **625**, 126934.
34 L. Zhang, S. Li, K. P. O'Halloran, Z. Zhang, H. Ma, X. Wang, L. Tan and H. Pang, *Colloids Surf. Physicochem. Eng. Asp.*, 2021, **614**, 126184.
35 Z. Yang, Y. Liu and J. Wang, *Chem. Eng. J.*, 2022, **427**, 131961.
36 H. Q. Ha, H. T. D. Nguyen, T. H. M. Pham, V. T. Pham and T. Truong, *Catal. Commun.*, 2018, **117**, 79–84.
37 L. Hu, J. Chen, Y. Wei, M. Wang, Y. Xu, C. Wang, P. Gao, Y. Liu, C. Liu, Y. Song, N. Ding, X. Liu and R. Wang, *J. Hazard. Mater.*, 2023, **442**, 130059.
38 M. Moayed Mohseni, M. Jouyandeh, S. Mohammad Sajadi, A. Hejna, S. Habibzadeh, A. Mohaddespour, N. Rabiee, H. Daneshgar, O. Akhavan, M. Asadnia, M. Rabiee, S. Ramakrishna and R. Luque, and M. Reza Saeb, *Chem. Eng. J.*, 2022, **449**, 137700.
39 C. Arul, K. Moulaee, N. Donato, D. Iannazzo, N. Lavanya, G. Neri and C. Sekar, *Sens. Actuators, B*, 2021, **329**, 129053.
40 N. Missaoui, H. Kahri and U. B. Demirci, *J. Mater. Sci.*, 2022, **57**, 16245–16257.
41 M. Sinnott, B. T. Kinsley, A. D. Jackson, C. Walsh, T. O'Grady, J. J. Nolan, P. Gaffney, G. Boran, C. Kelleher and B. Carr, *PLoS One*, 2015, **10**, e0122704.
42 N. Zhang, M.-X. Li, Z.-X. Wang, M. Shao and S. Zhu, *Inorg. Chim. Acta*, 2010, **363**, 8–14.
43 F. Wei, D. Chen, Z. Liang, S. Zhao and Y. Luo, *RSC Adv.*, 2017, **7**, 46520–46528.
44 N. A. Surib, A. Kuila, P. Saravanan, L. C. Sim and K. H. Leong, *New J. Chem.*, 2018, **42**, 11124–11130.
45 Y. Hou, L. Wang, G. Chen, Y. Liu, X. Miao, G. Wu, Z. Cao and Y. Zhang, *Ionics*, 2022, **28**, 3719–3729.
46 Z. Dong, Z. Mi, W. Shi, H. Jiang, Y. Zheng and K. Yang, *RSC Adv.*, 2017, **7**, 55504–55512.
47 N. Shooto, W. Donbebe, L. Sikhwivhilu, E. Dikio, F. Mtunzi and M. Maubane, *Dig. J. Nanomater. Biostruct.*, 2016, **11**, 425–434.
48 G. Wang, J. Wang, Z. Chen and J. Hu, *Int. J. Biol. Macromol.*, 2022, **206**, 232–241.

49 K. Karim, A. Lamaoui and A. Amine, *J. Pharm. Biomed. Anal.*, 2023, **225**, 115207.
50 I. Ortiz-Gómez, A. Salinas-Castillo, A. G. García, J. A. Álvarez-Bermejo, I. de Orbe-Payá, A. Rodríguez-Diéguez and L. F. Capitán-Vallvey, *Microchim. Acta*, 2017, **185**, 47.
51 P. Arul, N. S. K. Gowthaman, S. A. John and M. Tominaga, *Electrochim. Acta*, 2020, **354**, 136673.
52 Y. Sun, Y. Li, N. Wang, Q. Q. Xu, L. Xu and M. Lin, *Electroanalysis*, 2018, **30**, 474–478.
53 Md. A. Rashed, M. Faisal, J. Ahmed, S. A. Alsareii, M. Jalalah and F. A. Harraz, *J. Saudi Chem. Soc.*, 2022, **26**, 101480.
54 P. Arul and S. Abraham John, *J. Electroanal. Chem.*, 2017, **799**, 61–69.
55 Y. Xie, Y. Song, Y. Zhang, L. Xu, L. Miao, C. Peng and L. Wang, *J. Alloys Compd.*, 2018, **757**, 105–111.
56 S. Kim and A. Muthurasu, *J. Electroanal. Chem.*, 2020, **873**, 114356.
57 W. Pan, Z. Zheng, X. Wu, J. Gao, Y. Liu, Q. Yuan and W. Gan, *Microchem. J.*, 2021, **170**, 106652.
58 Y. Zhang, Y. Huang, P. Gao, W. Yin, M. Yin, H. Pu, Q. Sun, X. Liang and H. Fa, *Microchem. J.*, 2022, **175**, 107097.
59 L. Zhang, X. Ma, H. Liang, H. Lin and G. Zhao, *J. Mater. Chem. B*, 2019, **7**, 7006–7013.